Technical Paper

ISSN 1997-1400 Int. J. Pavement Res. Technol. 7(2):124-134

Design of a New Prefabricated Road Subsurface Drainage System

J. Norambuena-Contreras[1], E. Blanco-Fernandez[1], J.J. Del Coz Díaz[2], and D. Castro-Fresno[1+]

Abstract: Water flow through road structures is a topic of great interest in civil engineering, as water is one of the factors that most affects the hydraulic and mechanical behavior of road materials. Efficient design of subsurface drainage improves the performance of road pavement. Conventional drainage systems, such as trench drains may not be wholly effective in reducing water-related problems, and in fact, may inadvertently reduce pavement performance and service life. This can be because conventional drainage is projected in saturated conditions; however, most water flow near the surface occurs under unsaturated conditions. This paper presents an experimental study to design a new prefabricated prototype for the subsurface drainage of road pavements (SubDrain). SubDrain has been designed by using rapid prototyping Selective Laser Sintering (SLS) with powder polyamide material and experimental validation tests, with the aim to evaluate the mechanical and hydraulic behavior of the prototype. The results of this study show that the new prefabricated prototype is a potential technology solution to replace the conventional trench drain systems currently used in road projects. Findings in this study are limited to a prototype tested only under laboratory conditions.

DOI:10.6135/ijprt.org.tw/2014.7(2).124
***Key words**: Construction; Prefabricated; Rapid prototyping; Subsurface drainage; Water flow.*

Introduction

Water flow through road structures is a topic of great interest in civil engineering, as water is one of the factors that most affects the behavior of road materials. Therefore, an efficient design of the subsurface drainage using drainage systems improves the behavior of road pavements [1]. At present, the most frequently used method for road subsurface drainage is the trench drain system, which is the main component of road drainage worldwide, as shown in Fig. 1. Conventional trench drains consist of different materials: a drain pipe, normally a plastic pipe with diameters from 150 to 200 mm with grooves or perforations; a collector pipe with diameters larger than 300 mm or a geocomposite drain, wrapped in a porous mineral material (mineral material such as a rounded or crushed aggregate), protected by a filter material (usually a non-woven geotextile) and top sealed with an impervious material [2]. Besides, the geotextile is employed as a filter, which prevents the migration of fine soil particles into the drain and clogging. In addition, different materials have been used for the pipe of the trench drain, e.g., perforated or porous concrete, to PVC and fiberglass, the latter with grooves or perforations [3].

In their study on water flow into pavement, Stormont and Zhou [4] have shown that the trench drain is an important component in pavement drainage systems. However, conventional trench drains may not be wholly effective in reducing water-related problems, and in fact, may inadvertently reduce pavement performance and service life. Moreover, unsatisfactory results obtained in many road projects incorporating trench drain systems [5] cast doubts on the drainage efficiency and materials used in the construction of these systems, usually normalized by the different government road agencies of each country [6]. As a consequence, different studies [1- 8] related to subsurface drainage in road pavement structures and its assessment under field conditions conclude that the factor which contributes most to early pavement deterioration is the time required to drain the water entering base and subbase layers due to rainwater infiltration into the road.

Authors such as Wyatt and Macari [9] attributed this result to inadequate design of drainage elements. Conventional drainage (Fig. 1(a)) is projected in saturated conditions; however, most water flow near the surface occurs under unsaturated conditions. Additionally, different current studies [10] suggest that the performance of conventional drainage systems can only be understood if concepts of unsaturated flow are considered [7]. For example, coarse materials such as gravel and coarse sand are less conductive than finer-grained materials under most unsaturated conditions [4]. As a result, gravel soil (see Fig. 1(b)) may actually serve as an impediment to flow under the unsaturated conditions that exist within road pavement sections most of the time. Hence, an efficient design of the subsurface drainage using new drainage systems considering unsaturated flow principles can help to reduce the time required to drain the water. The appropriate design and correct installation of subsurface drainage systems are essential in the improvement of pavement durability. Thus, the development of new drainage systems as alternatives to the conventional trench drain represents a key advance in this field and can extend the knowledge about new designs, construction, and maintenance. In this context, Table 1 presents a critical review of the main studies developed on drainage systems in road pavements (surface and subsurface) in recent years. As shown in Table 1, there are still very few studies on the design of new technology solutions in subsurface drainage systems. Moreover, the most used shapes of sections are "U" and circle, followed by "T" and ovoid. According to the literature review, thermoplastic materials are the most commonly used (e.g.,

[1] GITECO Research Group. Civil Engineering School. Universidad de Cantabria. 39005 Santander, Spain.
[2] Department of Construction, EPSIG, University of Oviedo, 33204 Gijón, Spain.
[+] Corresponding Author: E-mail castrod@unican.es
Note: Submitted March 1, 2013; Revised September 2, 2013; Accepted November 18, 2013.

(a) (b)

Fig. 1. Conventional Drainage: (a) Trench Drain Under-construction and (b) Main Construction Materials Used.

polyethylene (PE), PVC, polypropylene (PP), and medium (MDPE) and high-density polyethylene (HDPE)) together with waterproof concrete or polymer concrete. However, manufacturing scale prototypes in these materials, at the design stage, is very expensive. This is due to the high cost of the moulds required to manufacture parts in series by conventional methods such as injection moulding, extrusion, or blow moulding. However, at present, these costs have started to be reduced by the development of new manufacturing technologies and rapid prototyping [11]. Rapid prototyping (RP) [12] is a term which embraces a group of new techniques for producing accurate parts directly from computer-aided design (CAD) drawings (.STL file) in a few hours, with little need for human intervention [13]. RP technologies are based on an additive process in which complex structures are constructed in a layer-by-layer manner according to a computer program implemented in a 3D printer or printing machine. Although there are different techniques of rapid prototyping [11, 14] (e.g., selective laser sintering (SLS), solid ground curing (SGC), laminated object manufacturing (LOM), three-dimensional printing (3DP), fused deposition modeling (FDM), solid creation system (SCS), solid object ultraviolet-laser plotter (SOUP), etc.), SLS techniques remain the most commonly used in engineering design and manufacturing industry as an intermediate step between planning and production to validate the usability of a new product [15, 16].

Therefore, this paper's objective is to develop a new prefabricated prototype for the subsurface drainage of road pavements by using a rapid prototyping technology and laboratory validation tests. To reach this objective, different tests such as the tensile and flexion characterization test, compression creep test, and a hydraulic behavior test using a 2D transparent tank, have been developed on test specimens. Finally, the different test specimens have been manufactured by using Selective Laser Sintering (SLS) with powder polyamide PA12.

Materials and Methods

New Prefabricated Prototype

Fig. 2 shows the preliminary design of new prefabricated prototype (SubDrain) analyzed in this paper. SubDrain is a prefabricated module that consists of a high-porosity deck with hexagonal cells wrapped up in a geotextile filter adhered by heat-melting along the contacts between the deck and the geotextile. Moreover, the deck has been attached to an open U-shaped collector channel which stands on four structural ribs open at the bottom to prevent flotation, forming a single body. In addition, it has two male-female joints at its ends for assembling to the following module. Finally, the SubDrain design presents the following characteristics:

1. High-strength design and anti-rollover structural stability. This is due to its deck design with hexagonal cells and rib beams at the base, see Fig. 2(a). The structural ribbed support also provided high stability to the module, supporting the load due to the soil weight on the prefabricated structure.
2. Adequate infiltration capacity and water drainage. Owing to its high-porosity deck and large U shaped collector channel. This open section collector channel can drain at flow rates equivalent to those of a conventional collector pipe with 300 mm diameter, considering an equivalent hydraulic section based on the rational hydraulic formulation of Manning and for a range of longitudinal installation slope between 0.5 and 5% (see SubDrain flow rates in Table 2). In addition, the flat deck design allows the installation of modular plastic geocellular units, increasing the infiltration capacity for higher depths of installation; see Fig. 2(a).
3. Easy transportation and on-site installation as a result of the component's low weight (less than 10 kg), and compact geometry. The installation is straightforward (Fig. 2(b)), as its two male-female joints enable the construction of an underground drain of any length (Fig. 2(c)). Hence, it expected that the module can be installed also in curved sections of roads; however, this has not been checked in this study. In addition, its design of deck with high porosity and adhered geotextile filter saves the installation of the conventional porous mineral material and geotextile filter extended into trench (Fig. 2(d)).

Powder Polyamide Material

Polyamide PA12 was used in this study for the preparation of test specimens by using Selective Laser Sintering (SLS) technology.

PA12 is a fine-powder of polyamide 12. Thus, PA12 presents a large difference between melting and crystallization points (~40℃) and a large enthalpy of fusion [17]. Therefore, its properties help to keep the temperature in the sintering chamber at a high level, resulting in low shrinkage on solidification and fairly good dimensional stability of the pieces using rapid prototyping technologies, such as selective laser sintering [16]. Polyamide PA12 was used in this technical study for the validation tests only, irrespective of the final

Table 1. Review of the Main Technology Solutions for Drainage Systems in Roadways.

Relevant Information about Patent					Shaped	Construction	Drainage
Inventor(s)	Year	Country	Number	Short Name	Section	Material	Type[b]
Hargett E.R.	1972	USA	US3645177(A)	Pavement Drainage System	U	Steel and Plastic	SD
Beanland N.S.	1981	UK	GB2069574(B)	Hollow Kerb Drainage Units	U	Concrete	SD
Thomann R. et al.	1986	USA	US4630962(A)	Drainage Channel with Locking Grate	U	Steel and Plastic	SD
Dahowski D.E.	1987	Canadian	CA1221043(A1)	Modular Drain System	Circle	Thermoplastic	SB-D
Ellis D.W.	1988	USA	US4793728(A)	Subsurface Water Drainage System	T	Polyethylene	SB-D
Sato I. et al.	1996	EP[a]	EP0721027(A1)	Drainage System for Use with Paved Road	C	Synthetic Fibers	SD
Gunter Ch.E.	1997	Germany	WO9720991(A1)	Drainage Channel and Associated Method	U	Thermoplastic	SD
Higashinaka T.	1998	Japan	JP10037286(A)	Receiving Frame for Draining Pavement	C	Concrete	SD
Ishida T. et al.	1998	Japan	JP10060810(A)	Channel Block for Draining Permeating Water	Circle	Concrete	SD
Kobayashi S. et al.	1999	Japan	JP11247113(A)	Partially Draining Road Pavement Structure	U	Concrete	SD
Maheara E.	1999	Japan	JP11222912(A)	Culvert Block for Draining Pavement	U	Thermoplastic	SD
Nattass N.	1999	Germany	WO9939056(A1)	Water Drainage Channel	C	Thermoplastic	SD
Becker A.R. et al.	1999	USA	US6000881	Trench Drain	U	Steel and Plastic	SD
Arakami A. et al.	2000	Japan	JP2000170239(A)	Structure of Drainage Channel Installation Pipe	Circle	Polymer Concrete	SD
Furukawa K.	2000	Japan	JP2000001806(A)	Drain-gutter Block	U	Polyethylene	SD
Hanamura S.	2000	Japan	JP2000129634(A)	Channel Block for Drainable Pavement	U	Thermoplastic	SD
Hatori T.	2000	Japan	JP2000129769(A)	Closed Side Ditch for Drainable Pavement	U	Thermoplastic	SD
Nakayama K., Akamatsu H.	2000	Japan	JP2000303546(A)	Draining Structure of Pavement	Circle	Concrete	SD
Gunter Ch.E.	2001	USA	US6170796(B1)	Mold and Associated Method for Making a Drainage Channel	Circle	Concrete	SD
Matsubayasi K.	2001	Japan	JP2001123518(A)	Drain Attached Pavement	Ovoid	Concrete	SD
Charlesworth J.K.	2002	USA	US2002057943(A1)	Kerb and Drainage Installation	Circle	Thermoplastic	SD
Fujita A.	2002	Japan	JP2002181247(A)	Water Conducting Pipe Buried in Permeable Pavement	Circle	Synthetic Fibers	SB-D
Fujita A. et al.	2002	Japan	JP2002061270(A)	Side Ditch Block and Draining Structure	Circle	Thermoplastic	SB-D
Ianniello P.J. et al.	2002	USA	US2002044842(A1)	Drainage System with Geosynthetic Structure	T	Polyethylene	SB-D
Sendai T.	2002	Japan	JP2002227111(A)	Channel Block	U	Thermoplastic	SD
Tanaka H. et al.	2002	Japan	JP2002364785(A)	Drain Structure	Circle	Plastic Resin	SB-D
Kusatake S.	2003	Japan	JP2003328424(A)	Side Ditch Block	Circle	Thermoplastic	SD
Matshusita M. et al.	2004	Japan	JP2004084457(A)	Drain block and Drainage Structure	Circle	Thermoplastic	SD
Moriya T. et al.	2004	Japan	JP2004332331(A)	Block and Drainage Structure of Pavement	L	Thermoplastic	SD
Sasaki K.	2004	Japan	JP2004285819(A)	Concrete Part Body for Road Surface Drainage	L	Concrete	SD
Akeda R.	2004	Japan	JP2004244911(A)	Drain Structure of Water Permeable Pavement	Circle	Concrete	SD
Kamishiro T., Moriya T.	2006	Japan	JP2006183404(A)	Boundary Block Structure Roadway	U	Thermoplastic	SD

[a]EP: European Patent. [b]SD: Surface drainage, and SB-D: Subsurface drainage.

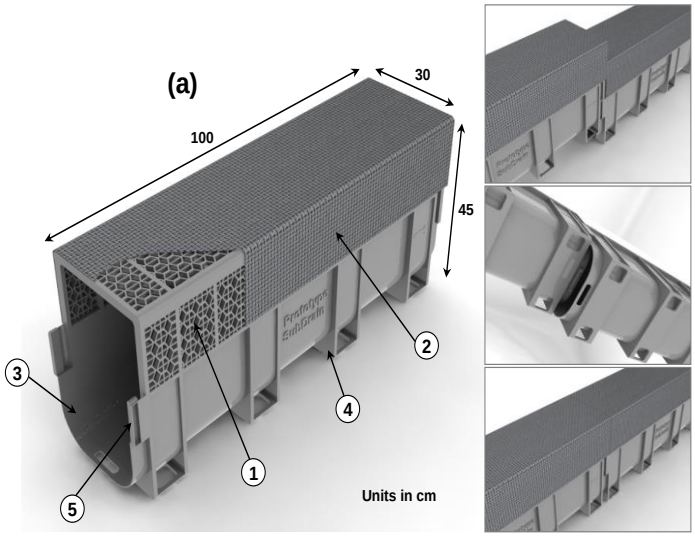

Fig. 2. New Prefabricated Prototype for Subsurface Drainage of Road Pavements: (1) Deck with Hexagonal Cells, (2) Adhered Geotextile Filter, (3) U-shaped Channel, (4) Structural Ribs, and (5) Male-female Joints.

manufacture material of the new prefabrication. Table 3 presents a summary of basic physical properties of polyamide PA12. These values can be considered as the standard average in the physical characterization of this type of material given by the technical catalogues.

Test Specimens Preparation

Fig. 3 shows a diagram of the manufacturing process developed. Basically, SLS technology uses a fine powder material (approx. 50 μm) which is heated with a CO_2 laser with a power in the range of 25 and 50 W, so that the grain surface tensions are overcome, making them to fuse together [13]. Before the powder is sintered, the entire bed is heated up to just below the material's melting point in order to minimize thermal distortion and facilitate fusion to the previous layer.

Therefore, each layer is drawn on the powder bed and the laser is used to sinter the material. Then, the bed is lowered and a powder-feed chamber is raised. Thus, a new covering of powder is spread by a counter-rotating roller; where the sintered material forms a part while the un-sintered powder remains in place to support the structure [12]. Although different powder materials exist, the materials most commonly used are polyamides, so the mechanical characteristics of the prototypes are, in some cases, even better than the models manufactured using moulds [16].

Finally, in order to obtain a prototype of greater size, SubDrain

Table 2. Sub Drain Flow Rates in (l/s) Calculated Using the Manning Formula.

Height Ratio (h/H), H=25cm 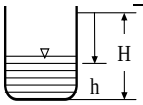	Longitudinal Slope of the Road (%)					
	0.5	1	1.5	2	3	5
0.1	4	5	6	7	9	12
0.2	13	18	22	26	31	41
0.3	26	36	44	51	63	81
0.4	40	57	70	81	99	128
0.5	56	79	97	112	138	178
0.6	73	103	126	145	178	230
0.7	90	127	155	179	220	283
0.8	107	151	185	214	262	338
0.9	125	176	216	249	305	394
1.0	142	201	247	285	349	450

[a]Manning coefficient used: 0.006.

was printed in the vertical axis of the machine (Fig. 3(a)), providing a 50% scale (1:2) in relation to the full-scale prototype; in the machine, the scale was 1:1.8 exactly. In addition, test samples for the mechanical characterization of polyamide were made at a real scale, with dimensions according to European standards [18, 19]. Moreover, a section of the prefabricated system at a scale of 1:2 was also manufactured for the hydraulic functionality study.

Mechanical Characterization of Polyamide

With the aim to determine the mechanical properties of the polyamide PA12 sintered vertically, a mechanical characterization including flexural and tensile tests was performed in laboratory, see Fig. 4. The tests were carried out according to the indications of European standards. In addition, all test samples were tested in dry conditions. Flexural tests were performed on five samples with dimensions 80×10×4 mm according to the standard EN ISO 178 [18]. The sample shape and experimental test arrangement are shown in Fig. 4(a). The test methodology consisted of placing each of the samples on two simple supports, applying a point load at the midpoint at a constant rate displacement of 2 mm/min. Both the force applied and the midpoint deflection were measured and recorded in short time intervals. Finally, flexural properties: stress, strain, and flexural modulus, have been determined according to the formulation described in European standard [18].

Furthermore, tensile test was performed according to the standard EN ISO 527-2 [19]. The test samples with the standard dimensions and failure state of the experimental test are shown in Fig. 4(b). Additionally, "T" strain gauges have been attached in some of the

Table 3. Physical Properties of Polyamide PA12 in Powder and Sintered Conditions.

PA12 state	Property	Measurement Method/Standard DIN or ISO	Unit	Value
Powder	Bulk Density	DIN 53466	g/cm^3	> 0.430
	Grain Size D_{10}	Laser Diffraction (Malvern Mastersizer)	μm	40
	Grain Size D_{50}		μm	58
	Grain Size D_{90}		μm	90
Sintered	Density	EOS-Method	g/cm^3	0.90-0.95
	Coefficient of Linear Thermal Expansion	DIN 53752-A	$\times 10^{-4}$ /K	1.09

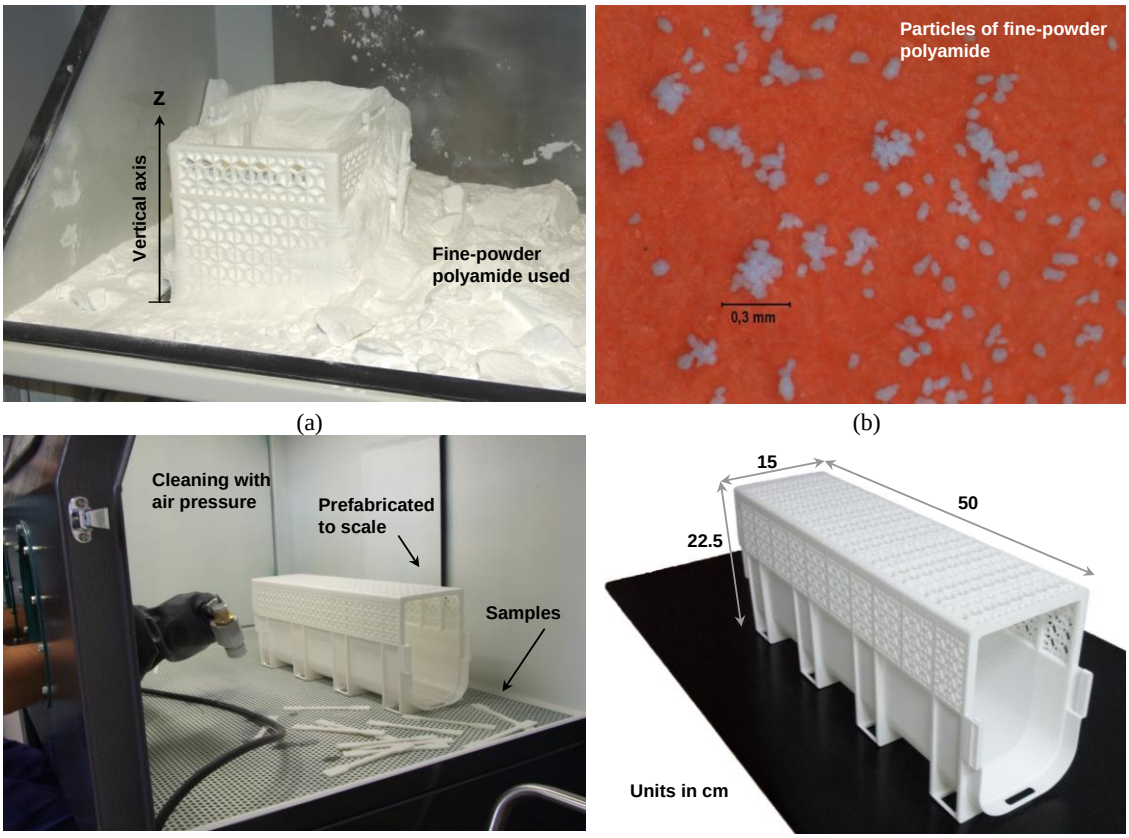

Fig. 3. Rapid Prototyping of Test Specimens by Selective Laser Sintering Technology: (a) Vertical Printing of Prefabricated to Scale, (b) Powder Polyamide Material, (c) Cleaning Process of Tests Specimens Using Air Pressure, and (d) Prefabricated to Scale.

Fig. 4. Mechanical Characterization on Polyamide Test Samples: (a) Flexural Test, and (b) Tensile Test.

samples to measure longitudinal and transversal strain, in order to determine Poisson's ratio. The elongation was also measured with an optical extensometer for all specimens. The test methodology consisted in placing each sample in a universal testing machine, securing the ends of the sample to the jaws using a pressure of 50 bar (5 MPa), and then separating the jaws at a constant rate. The surfaces of the clamps were wrapped with polyurethane to the ends of the samples. A constant rate displacement of 100 mm/min was applied until reaching failure. Specimen length (distance between clamps) was 115 mm. Moreover, the test samples were classified in two groups: samples without gauge (5 units) and samples with gauges (3 units). For this reason, longitudinal strain was measured on samples without gauges using an optical extensometer. In addition, for samples with strain gauges, longitudinal strain was measured with both gauges and optical extensometer, while transversal strain was measured only with the gauges. Finally, tensile elastic properties—stress-strain relationship, Young's Modulus, and Poisson's ratio—have been determined according to the formulation described in the European standard [19].

Compression Creep Test on Prefabricated Prototype

Considering that polymer materials, as sintered Polyamide PA12 [16], exhibit time dependent behavior, a compression creep test at a temperature of 22℃ was performed on a SubDrain prototype to scale. Fig. 5 shows a schematic diagram of the creep test developed. Thus, with the aim to assess the range of stress level due to earthfill load on the prefabricated to scale (applied force); the service load was calculated using Marston's theory for loads on buried flexible pipes [20].

Marston trench load theory takes into account vertical loads due to the earthfill at the top along with lateral loads due to natural soil pressures, according to the Rankine's theory. Marston's theory also considers the shear stresses between natural soil and the earthfill wall to reduce the vertical load applied by the earthfill. Moreover,

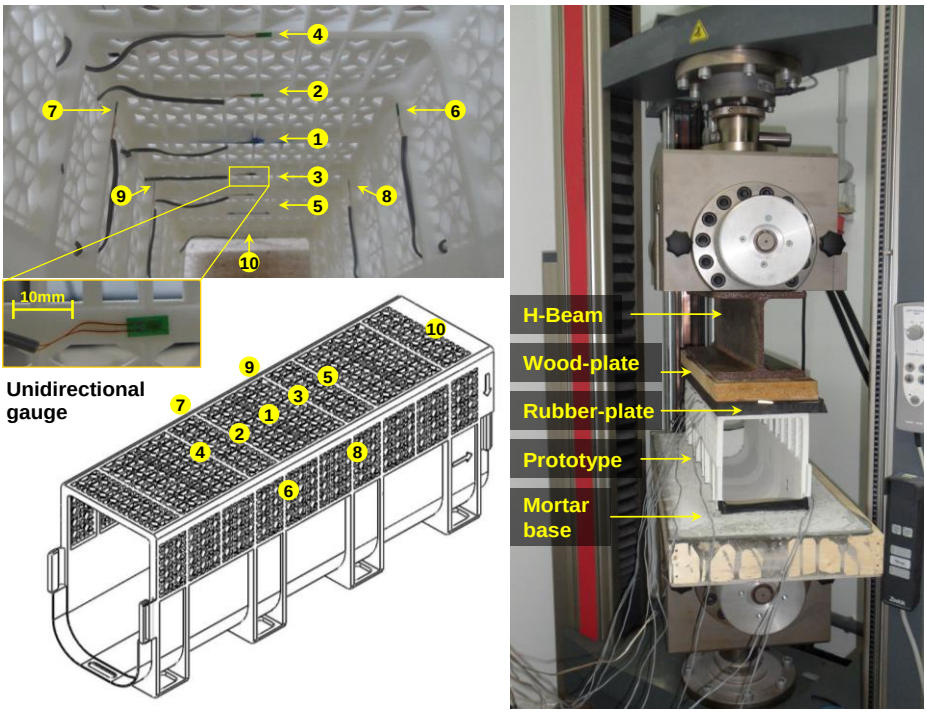

(a) (b)

Fig. 5. Compression Creep Test: (a) Unidirectional Gauge Positions, and (b) Schematic of the Test.

the application of the Marston trench load has been used in several European codes [21]. Thus, the analysis of results considering an earthfill soil with a specific weight of 20 kN/m^3 (e.g., coarse gravel soil), trench width of ~0.4 m, 3 m earthfill depth, a friction angle of the natural soil of 33º, and a Marston coefficient friction product of 0.19, yields a service load of 8 kN per meter of trench. Considering only the hexagonal cells on the top surface of a 1m length prefabricated module, a net area of 0.125 m^2 has been considered. Therefore, the service pressure applied on top of a prefabricated module was 64 kPa. Finally, this load adequately scaled to our prototype and, considering a net area of application of 0.038 m^2, leads to a force value of 2.4 kN. Therefore, the compression creep test was performed on a SubDrain prototype sample prepared in similar conditions of installation. Thus, the prototype was embedded into a 6 cm thick prefabricated rectangular mold filled with a self-compacting rapid hardening mortar. The test consisted of placing the sample in a universal machine and applying an evenly distributed load of 64 kPa, which for the sample dimensions reached 2.4 kN. In addition, a rubber sheet, a wooden base, and a steel T-beam were placed at the top of the sample, to accomplish an evenly distributed force.

Thus, those accessories supplied an initial load of 258 N. Subsequently, a ramp load was applied for approximately 1 minute until reaching 2.4 kN, according to the recommendations of the European standard EN ISO 25619-1 [22]. So, once the force of 2.4 kN was reached, it was maintained constant during the compression creep test during a time of 813,708 seconds (9 days). Finally, 10 unidirectional gauges were placed at various points in the sample in order to measure the strains in the SubDrain to scale-tested (see distribution in Fig. 5(a)). So, the criterion for selection of the measurement points was to consider the 10 locations with highest longitudinal strains given by the output of finite element analysis. Moreover, symmetrical positions were selected to obtain average strain values and correct possible asymmetries in the load application.

Hydraulic Behavior Study

In order to study the hydraulic behavior of the new prefabricated prototype (SubDrain), a hydraulic qualitative test using a 2D transparent tank with an original granular porous media inside [23] has been developed by the Materials Technology and Environment Research Group of the Polytechnic University of Madrid (TEMATMA-UPM) in collaboration with the Construction Technology Research Group of the University of Cantabria (GITECO-UC). Fig. 6 shows a schematic diagram of the hydraulic behavior test.

Basically, the hydraulic qualitative test consisted of applying a known water volume through two by-pass valves located on the sides of a transparent tank, simulating a sub-horizontal flow through a porous medium, which was previously confined by pressure. This confining pressure was applied through a system of vertical bars located at the top of the tank, see Fig. 6. The simulation of the porous media wrapped onto the prefabricated section, covered with a geotextile filter, was set up using transparent soil technology. This technology has been developed in the published works by Iskander et al. [23- 26], referent to modeling with transparent soils applied to the geotechnical engineering, e.g., modeling soil structure interaction and multi-phase flow.

This transparent soil consists of a water-based transparent synthetic polymer used to reproduce a two-phase flow with water as the saturation liquid [25]. The physical principle of modeling using transparent soils is based on refractive index of two media, a granular solid material and a void saturation liquid [23]. This

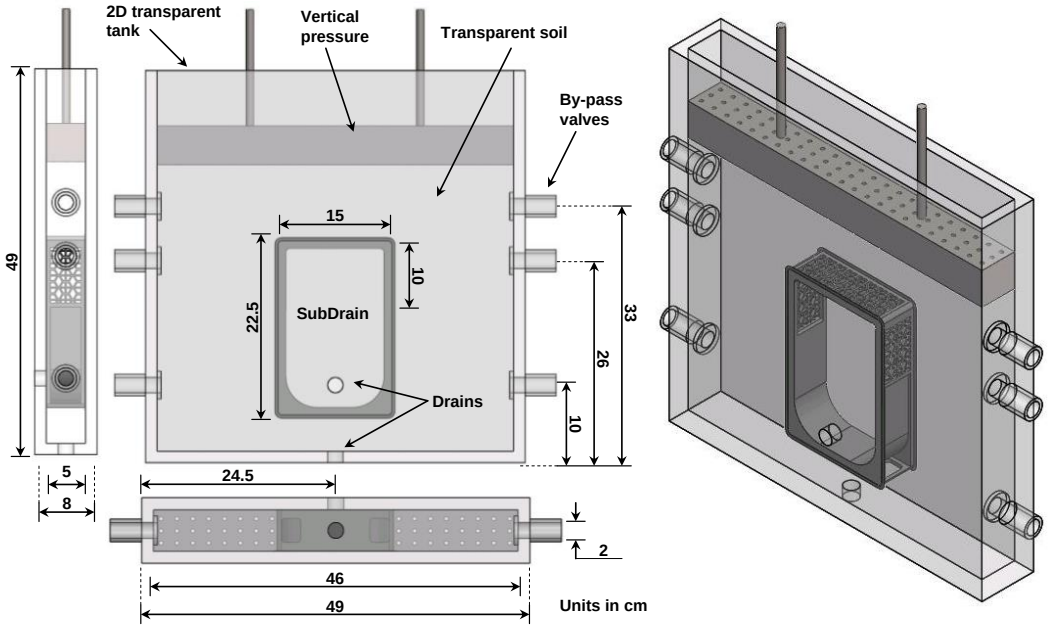

Fig. 6. Preliminary Design of Hydraulic Behaviour Test in SubDrain.

Table 4. Properties of Transparent Soil and Geotextile Filter Used.

Material Type	Description	Symbol	Unit	Value[a]
Transparent Soil (Modified from [23])	Hydraulic Conductivity	k_s	cm/s	5×10^{-2}
	Particle Size (Pass. 50%)	D_{50}	mm	20
	Refractive Index	n	–	1.33
	Vertical Confining Pressure Applied in Test	σ_c	kPa	5
Geotextil Filter (According to [27] and [28])	Vertical Permeability (Δh=50 mm)	k_v	mm/s	130
	Opening Size	O_{90}	μm	120

material exhibits transparency under completely saturated conditions. Therefore, this hydraulic qualitative test provided a real-time observation of the infiltration capacity and drainage of the new prefabricated prototype. Finally, Table 4 shows the properties of the transparent soil and the hydraulic properties of the geotextile filter used in the test.

Results and Discussion

Mechanical Characterization of Polyamide

Table 5 and Table 6 include the results of mechanical characterization on sintered samples of polyamide. Concerning flexural properties that are shown in Table 5, the experimental results show that the average values of stress, strain, and modulus were 63.96 MPa, 7.41%, and 1869 MPa respectively. In addition, good repeatability was observed in the tests, as the coefficient of variation ranged between 0.04 and 0.10. Moreover, the tensile properties registered in Table 6 showed different results in the case of the elastic modulus. In the group of samples without gauge, the experimental results obtained show that the average values of stress, strain, and elastic modulus were 46.125 MPa, 11.34 %, and 1404 MPa, respectively. However, for the group of samples with gauge, the average value of the elastic modulus was 1615 MPa. Elastic modulus was calculated for a stress range from 5 to 10 MPa. The average tensile yield strength estimated at 0.2% and the average ultimate tensile strength were 26 and 46 MPa, respectively; and the average value of Poisson's ratio was 0.46. Therefore, these results can be considered as the standard average values in the mechanical characterization of vertically sintered polyamide samples, complementary to the study developed by Seltzer et al. [16], referent to the fracture behavior of PA12 composites processed by

Table 5. Results of Flexural Properties for Vertically Sintered Polyamide Samples.

Samples	Flexural Properties		
	Stress (MPa)[a]	Strain (%)[a]	Flexural Modulus (MPa)
Average	63.96	7.41	1869
Standard Deviation	2.83	0.35	191
Coeff. of Variation	0.04	0.05	0.10

[a] Ultimate strength.

Table 6. Results of Tensile Properties for Vertically Sintered Polyamide Samples.

Samples	Tensile Properties				
	Samples Without Gauge			Samples with Gauge	
	Stress (MPa)[a]	Strain (%)[a]	Elastic Modulus (MPa)	Elastic Modulus (MPa)	Poisson's Ratio
Average	46.125	11.34	1404	1615	0.46
Standard Deviation	0.76	1.60	373.81	225	0.03
Coeff. of Variation	0.02	0.14	0.27	0.14	0.06

[a] Ultimate strength.

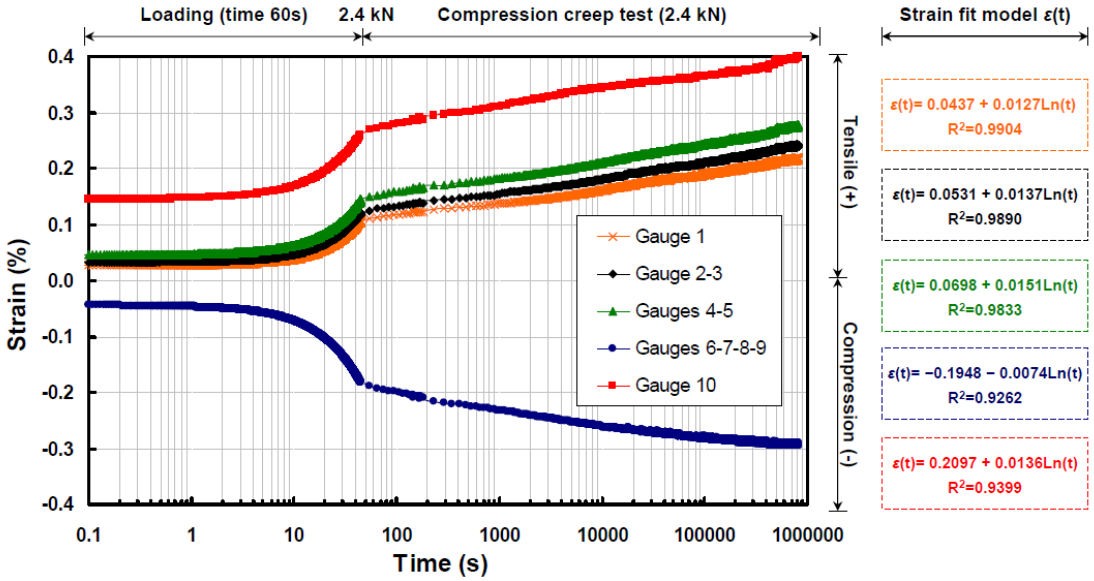

Fig. 1. Compression Creep Test Results at a Temperature of 22℃.

selective laser sintering. However, these characterization values could be slightly different if other sintering directions were used.

Long Term Performance of the Prefabricated

Fig. 7 shows the average strain values measured by the gauges over time in a prototype sample at a temperature of 22℃. This figure shows that gauges 1 to 5 and 10 developed positive strains (tensile), while gauges 6 to 9 showed negative strains (compression), as expected. In addition, the strain curves show a logarithmic behavior that can be fitted by the following equation $\varepsilon(t) = C1 + C2 \ln(t)$. The best strain fit model for each of the gauge groups and their correlating coefficients (R^2) can be observed in Fig. 7. Additionally, experimental results measured during creep for a testing time of approximately 9 days showed low values of strain, demonstrated by the low creep slope values (C2) that ranged from 0.0074 (gauges 6-7-8-9) to 0.0127 (gauge 1). Finally, the long-term strain values for the new prefabricated prototype sintered in polyamide PA12 have been very low, not reaching the ultimate tensile strength (11%) in years. Therefore, these results have shown that the design of the new prefabricated prototype has acceptable resistance to strain-compression over a long time, considering that polymer materials (as sintered Polyamide) exhibit time-dependent behavior, i.e., the stress and strain induced when a load is applied are a function of time.

Hydraulic Behavior of the Prefabricated

Fig. 8 shows snapshot results of the hydraulic simulations carried out on the 2D transparent tank. The hydraulic performance results of the new prefabricated prototype show a good infiltration capacity due to the design of its high-porosity deck. Additionally, the simulation of the sub-horizontal flow through a porous medium was also carried out using two by-pass valves fitted to the sides of a transparent tank. For this reason, the results show water flow simulation and saturation lines under transient (Fig. 8 (a)) and steady-state (Fig. 8 (b)) conditions.

Moreover, the granular porous media used in the hydraulic simulations showed transparency under completely saturated conditions and partial transparency in unsaturated conditions. Therefore, this experimental test can be potentially used to study the capillary barrier effect [29] in the contour of the high deck, due to abrupt changes of porosity between the porous media and geotextile filter. In this context, Richardson [30] found that the interface between soil and geotextile acted as a capillary barrier causing failures due to the buildup water above the geotextile. For example, Fig. 9 shows a conceptual test carried out in this study in order to model the capillary barrier effect on nonwoven geotextile samples tested under dry conditions. These results prove that nonwoven geotextiles can act as a capillary barrier; however, a minimum height water pressure must be reached to achieve a capillary break effect into the test specimen. A complete study on the hydraulic

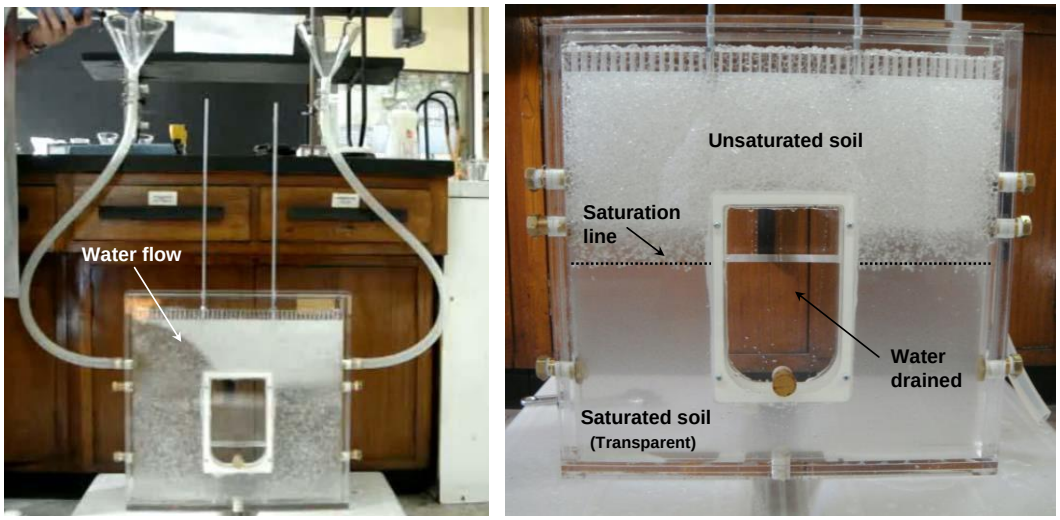

(a) (b)

Fig. 8. Graphical Results of the Hydraulic Simulations in the 2D Transparent Tank: (a) Transient Conditions, and (b) Steady-state Condition.

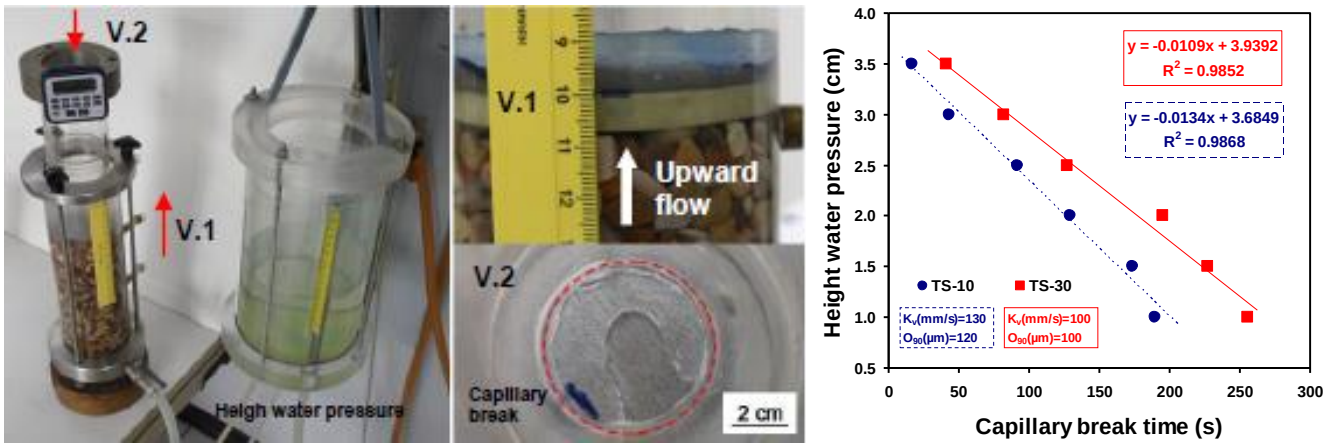

(a) (b)

Fig. 9. (a) Capillary Barrier Test on Nonwoven Geotextile Samples, and (b) Height Water Pressure Versus Capillary Break Time Measured on Two Different Geotextiles.

behavior of nonwoven geotextiles under unsaturated conditions has been developed by Asanza [31]. Finally, the TEMATMA-UPM Group is performing further research on the aforementioned hydraulic qualitative model (Fig. 6) in order to develop a solid scientific methodology based on the use of transparent soil applied to the study of drainage problems in road materials, considering that the first modeling has been successfully made by introducing the prefabricated prototype SubDrain (Fig. 8). Therefore, future numerical results will include the hydraulic simulations developed as part of this experimental research.

Conclusions

This paper presents the development of a new type of prefabricated prototype (SubDrain) for subsurface drainage of road pavements using a rapid prototyping technology and experimental validation tests. The main results of this study show that the new prefabricated prototype is a potential technology solution to replace the conventional trench drain systems currently used in road projects. However, to implement this technology solution effectively, the new prefabricated system solution needs to be tested in the field to evaluate installation procedures and the effectiveness of the system fabricated using similar materials to the ones used in the prototype SubDrain. Thus, the following remarks can be made based on this research:

- The preliminary design of a new prefabricated prototype tested only under laboratory conditions presents advantages in long-term mechanical strength, structural stability anti-rollover, and a good infiltration capacity and drainage.
- Rapid prototyping technology via Selective Laser Sintering with powder polyamide PA12 has proven to be a high-quality technology for the manufacture of prototypes with mechanical characterization purposes in laboratory. Moreover, results of the mechanical characterization on samples of polyamide PA12 can be considered as the standard average values in the mechanical resistance to tensile and flexural of polyamide material sintered in vertical direction.
- The results of this work show that the hydraulic laboratory scale model can be potentially used to study the capillary barrier effect in the contour of the high deck, due to abrupt

changes of porosity between the porous media and geotextile filter, considering that the first modeling has been successfully made by using the prefabricated prototype developed in this technical study.

Acknowledgments

The authors wish to acknowledge the support provided by the Materials Technology and Environment Research Group of the Polytechnic University of Madrid (TEMATMA-UPM), and the GITECO Research Groups and LADICIM of the University of Cantabria, Spain. They would also like to thank the Laboratory of Geosynthetics of the University of Cantabria and the company Dragados in Spain. Finally, the first author would also like to thank the FPU Programme of the Spanish Ministry of Education, Culture and Sport.

References

1. Canelon, D.J., and Nieber J.L. (2009). *Final Report: Evaluating Roadway Subsurface Drainage Practices, Department of Bioproducts and Biosystems Engineering.* University of Minnesota. Minnesota: Minnesota Department of Transportation, p.139.
2. Koerner, G.R., Koerner, R.M., and Wilson-Fahmy, R.F. (1996). Field Performance of Geosynthetic Highway Drainage Systems, *Journal of Engineering and Applied Sciences*, No. 1281, pp. 165-181.
3. Norambuena-Contreras, J. (2013). *Hydraulic and Mechanical Behaviour of Materials Used in Road Pavement Construction.* Ph.D. Thesis, University of Cantabria, Santander, Spain.
4. Stormont, J.C., and Zhou, S. (2005). Impact of Unsaturated Flow on Pavement Edgedrain Performance, *Journal of Transportation Engineering*, 131(1), pp. 46-53.
5. Christopher, B.R., and McGuffey, V.C. (1997). *Pavement Subsurface Drainage Systems. NCHRP Synthesis of Highway Practice 239*, Transportation Research Board, National Research Council, Washington, DC, USA.
6. Fleckenstein, J., and Allen, D. (2000). *Development of a Performance-based Specification (QC/QA) for Highway Edgedrains in Kentucky*, ASTM Spec. Technical Publication, No. 1390, pp. 64-71.
7. Norambuena-Contreras, J., Arbat, G., García Nieto, P.J., and Castro-Fresno, D. (2012). Nonlinear Numerical Simulation of Rainwater Infiltration through Road Embankments by FEM, *Applied Mathematics and Computation*, No. 219, pp. 1843-1852.
8. Fleckenstein, J., and Allen, D. (1996). Evaluation of Pavement Edgedrains and their Effect on Pavement Performance, *Transportation Research Record*, No. 1519, pp. 28-35.
9. Wyatt, T.R., and Macari, E.J. (2000). Effectiveness Analysis of Subsurface Drainage Features Based on Design Adequacy. *Transportation Research Record*, No. 1709, pp. 69-77.
10. Birgisson, B., and Roberson, R. (2000). Drainage of Pavement Base Material: Design and Construction Issues. *Transportation Research Record*, No. 1709, pp. 11-18.
11. Chua, C.K., Chou, S.M., and Wong, T.S. (1998). A Study of the State-of-the-Art Rapid Prototyping Technologies, *International Journal of Advanced Manufacturing Technology*, 14(2), pp. 146-152.
12. Pham, D.T., and Gault, R.S. (1998). A Comparison of Rapid Prototyping Technologies, *International Journal of Machine Tools and Manufacture*, 38(10-11), pp. 1257-1287.
13. Peltola, S.M., Melchels, F.P.W., Grijpma, D.W., and Kellomäki, M. (2008). A Review of Rapid Prototyping Techniques for Tissue Engineering Purposes, *Annals of Medicine*, 40(4), pp. 268-280.
14. Dickens, P.M. (1995). Research Developments in Rapid Prototyping. *Proceedings of the Institution of Mechanical Engineers*, Part B, Journal of Engineering Manufacture, 209(B4), pp. 261-266.
15. Kettner, M., Schmidt, P., Potente, S., Ramsthaler, F., and Schrodt, M. (2011). Reverse Engineering-Rapid Prototyping of the Skull in Forensic Trauma Analysis, *Journal of Forensic Sciences*, 56(4), pp. 1015-1017.
16. Seltzer, R., de la Escalera, F.M., and Segurado, J. (2011). Effect of Water Conditioning on the Fracture Behavior of PA12 Composites Processed by Selective Laser Sintering, *Materials Science and Engineering*, A, 528(22-23), pp. 6927-6933.
17. Tontowi, A.E., and Childs, T.H.C. (2001). Density Prediction of Crystalline Polymer Sintered Parts at Various Powder Bed Temperatures, *Rapid Prototyping Journal*, No. 7, pp. 180-184.
18. UNE-EN ISO 178. (2003). Plastics. Determination of Flexural Properties, May 2003.
19. UNE-EN ISO 527-2. (1997). Plastics. Determination of Tensile Properties. Part 2: Test Conditions for Moulding and Extrusion Plastics, January 1997.
20. Marston, A. (1930). *The Theory of External Loads on Closed Conduits in the Light of the Latest Experiments.* Bulletin No. 96, Iowa Engineering Experiment Station, Iowa State College. Ames, Iowa, USA.
21. McGrath, T.J., Moore, I.D., and Hsuan, G.Y. (2009*). Updated Test and Design Methods for Thermoplastic Drainage Pipe*, NCHRP Rep. No. 631, Transportation Research Board, Washington, DC, USA.
22. UNE-EN ISO 25619-1. (2009). Geosynthetics. Determination of Compression Behaviour. Part 2: Determination of Short-term Compression Behaviour, March 2009.
23. Fernández Serrano, R., Iskander, M., and Tabe, K. (2011). 3D Contaminant Flow Imaging in Transparent Granular Porous Media. *Géotechnique Letters*, 1(3), pp. 71-78.
24. Iskander, M., Lai, J., Oswald, C., and Mannheimer, R. (1994). Development of a Transparent Material to Model the Geotechnical Properties of Soils. *ASTM Geotechnical Testing Journal*, 17(4), pp. 425-433.
25. Iskander, M. (2010). *Modelling with Transparent Soils: Visualizing Soil Structure Interaction and Multi Phase Flow, Non-Intrusively.* Springer Series in Geomechanics and Geoengineering. Springer-Verlag, Berlin.
26. Lo, H., Tabe, K., Iskander, M., Yoon, S. (2010). A Transparent Water-Based Polymer for Simulating Multiphase Flow,

Geotechnical Testing Journal, 33(1), pp. 1-13.
27. UNE-EN ISO 11058. (2010). Geotextiles and Geotextile-Related Products. Determination of Water Permeability Characteristics Normal to the Plane, Without Load, July 2010.
28. UNE-EN ISO 12956. (2010). Geotextiles and Geotextile-Related Products. Determination of the Characteristic Opening Size, July 2010.
29. Stormont, J.C., and Anderson, C.E. (1999). Capillary Barrier Effect from Underlying Coarse Soil Layer. *Journal of Geotechnical and Geoenvironmental Engineering: ASCE*, 125(8), pp. 641-648.
30. Richardson, G.N. (1997). Fundamental Mistakes in Slope Design. *Geotechnical Fabrics Report*, 15(2), pp. 15-17.
31. Asanza, E. (2009). *Determination of the Friction Characteristics within the Soil-geotextile Interface at Different Suctions with Two Novel Laboratory Devices*. Ph.D. Thesis, Polytechnic University of Madrid, Madrid.